DOI: 10.13009/EUCASS2017-186

Subscale hypersonic free flight dynamics of HEXAFLY-INT EFTV + ESM (multibody separation)

Chris Kennell, Bodo Reimann**, Rishabh Choudhury***, David Buttsworth***, Andrew Neely**

**UNSW Canberra*
Canberra, Australian Capital Territory, Australia, 2600.

***DLR*
DLR, Institute of Aerodynamics and Flow Technology, 38108 Braunschweig, Germany

****University of Southern Queensland*
Toowoomba, Queensland, Australia, 4350.

Abstract

This study investigates the separation dynamics of the HEXAFLY-INT hypersonic glider and its attitude control module that is to be released prior to the flight experiment. Both experimental and numerical techniques are utilised. With regard to experiments, dynamically scaled down models with on-board accelerometers and gyroscopes are released into Mach 6 test gas and 'fly' unconstrained within the inviscid flow core. Dynamic behaviour was sought to be replicated using 3D printed models with a similar mass distribution. Numerical studies have been conducted using the DLR Tau coupled CFD/RBD solver. Both experimental and numerical trajectories of the module were compared and similar separation trends were observed throughout.

Nomenclature

a = Speed of sound (m/s)
I = Moment of inertia (kg m^2)
l = Length (m)
M = Mach number
m = mass (kg)
n = Scaling factor
P = Pressure (Pa)
T = Temperature (K)
U = Velocity (m/s)
υ = Kinematic viscosity (m^2/s)
ρ = Density (kg/m^3)
μ = Dynamic viscosity (Pa s)
γ = Ratio of specific heats

Subscript

∞ = Freestream Value
f = Fluid

DOI: 10.13009/EUCASS2017-186

1. Introduction

Traditionally, wind tunnel experiments are performed on models that are mounted on a sting, with measurements taken through a strain gauge force balance [1]. However due to the impulsive nature of hypersonic test facilities, useful flow durations are in the order of milliseconds. This can make force balance measurements challenging to resolve. The sting itself is also a drawback to this type of experiment as it will influence the flow field around the model, affecting the validity of the results obtained.

Due to these difficulties, the technique of 'instrumented free flight' has been developed. Scaled models are released and are free to move within the flow unconstrained, allowing dynamic effects to be studied. These models are instrumented with an on-board inertial measurement unit (IMU) consisting of a 3 axis accelerometer and a 3 axis gyroscope. Data from these sensors is transmitted wirelessly, post-test, through a Bluetooth connection to a receiving terminal located outside of the facility. Measurements of acceleration allow for direct calculation of lift and drag. This provides more accuracy than high-speed image analysis, which derives accelerations from displacements that must be differentiated twice, introducing uncertainty into the values. The effectiveness of this technique has been demonstrated on hemispherical-nosed cylinders [2] and later refined such that it could be applied to actual vehicle geometries [3, 4]. This technique also provides the ability to study inherently dynamic phenomena such as the separation behaviour of multiple bodies [5], which will be the focus of the current study with application to the HEXAFLY-International flight test project.

2. HEXAFLY-INT

2.1 Project Overview

High-speed civil transportation has seen a growth in interest over recent years, with several innovative conceptual designs put forward. These designs have the potential to dramatically increase the cruise range efficiency in the high supersonic and hypersonic flow regimes. This is achieved through the use of high lift airframes coupled with efficient air-breathing engines.

UNSW Canberra, along with various other partners from Europe, Russia and Australia, is contributing to the development of the HEXAFLY-INT (High-Speed Experimental Fly Vehicles - INTernational) vehicle within the 7th Framework program of the European Commission, led by the European Space Agency (ESA). This project will culminate in a test flight of a hypersonic glider within the atmosphere. Multiple experimental and numerical studies are being conducted by partners to validate and optimise design concepts. This project builds on previous work developed in previous projects HEXAFLY, LAPCAT I & II, ATLLAS I & II. [6,7,8]

2.2 Vehicle Configuration and Mission Profile

The Experimental Test Flight Vehicle (EFTV), shown in Figure 1, is a hypersonic waverider inspired glider. It has a length of 3.29 m and a wing span of 1.24 m. The wings have an 80 degree sweep angle along with a negative 14 degree dihedral angle. There are two ailerons at the trailing edge of these wings to allow for active control during the flight. To assist passively with lateral control there are also two fixed vertical fins on the top of the vehicle. For further technical details please consult [9, 10].

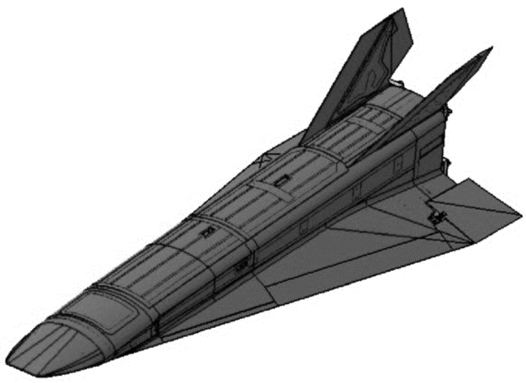

Figure 1: Experimental Test Flight Vehicle (EFTV) [9]

DOI: 10.13009/EUCASS2017-186

Figure 2 shows an illustration of the key phases of the test flight.

1. A VS43 Brazilian sounding rocket launches the payload (EFTV + ESM)
2. Rocket motor burnout
3. Ejection of the nose cone covering the payload
4. Attitude alignment of booster + payload
5. Release of payload (90 km)
6. Repositioning of EFTV using cold gas jets with the ESM
7. ESM release
8. EFTV pull up manoeuvre
9. Flight Experiment (controlled cruise @ M~7-8)
10. Touch down

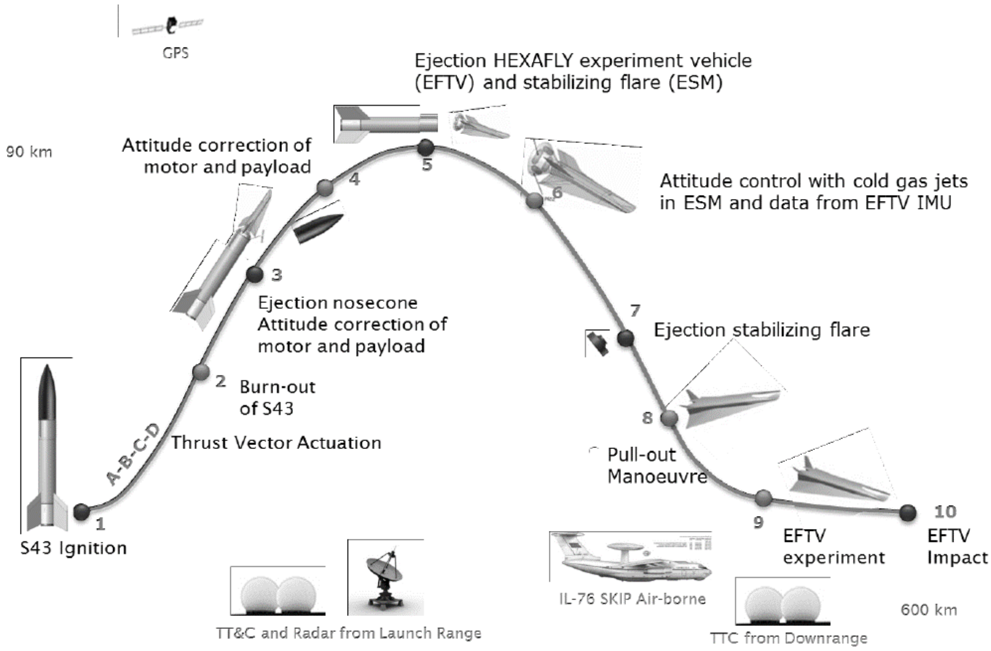

Figure 2: Flight Sequence Profile [9]

2.3 Experimental Service Module (ESM)

The Experimental Service Module (ESM) is attached to the rear of the EFTV and is used to control the attitude of the payload following its release from the booster. This is achieved by utilising IMU data to control a system of cold gas thrusters (CGS). Once the EFTV has been positioned such that it can be controlled solely by use of its own control surfaces, the ESM will be released and the pull up manoeuvre is performed. This is expected to occur within an altitude range of approximately 40 – 60 km. A schematic of the ESM is shown in Figure 3.

The release of the ESM from the EFTV is one of the most critical periods of the flight. If the ESM were to impact upon the EFTV upon release it could lead to damage of the main vehicle and potential failure of the mission. Ground testing plays an important role in assessing the separation dynamics and providing a benchmark for validating numerical predictions of the separation at other conditions.

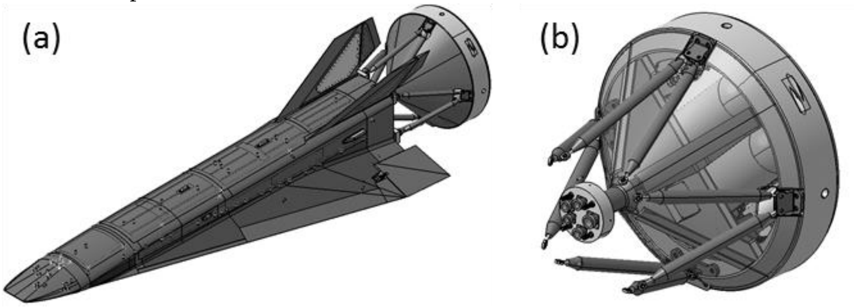

Figure 3: (a) EFTV + ESM (b) Standalone ESM [10]

DOI: 10.13009/EUCASS2017-186

3. Scaling Methodology

Replicating the dynamic behaviour of this separation on subscale models requires certain non-dimensional groups to be matched in order to maintain similitude between the experiments and the atmospheric flight. The scaling requirements for dynamic similitude of an unsupported rigid body in compressible flow are presented by [11] and shown in Table 1. These relations are derived from dimensional analysis of the parameters of interest, both of the flow and the model. Theoretically, if all of these conditions are met, the subscale model behaviour will exactly mimic that of the full-scale version. However, when conducting experiments, real world limitations need to be accepted. Constructing a model that fulfils the requirements can be challenging. Even if this is achieved, finding a test facility that can generate the correct flow conditions can also pose difficulties (especially in hypersonics). Non-dimensional flow parameters of significance are Reynolds number, Froude number and Mach number.

Reynolds number is the ratio of inertial to viscous forces in the flow. This plays an important role in defining the state of the boundary layer around the model. The component of viscous drag experienced by the model can be greatly affected by the flow regime encountered and the location of any regions of boundary layer transition and separation. The high flow velocities in hypersonic testing results in high shear stresses on the surface of the model, so a mismatch could have a significant effect.

Froude Number is the ratio of inertial and gravitational forces. This parameter was originally conceived as a similitude requirement for pressure coefficients on full scale and model scale ships. However, its importance also extends to other manoeuvring vehicles. Matching Froude number is important in accurately replicating turning motions, as it is essential for the acceleration due to gravity to be similar to lift and drag acceleration components generated by the surface pressure distribution.

Mach number, the ratio of flow velocity to the velocity of the speed of sound, is clearly a crucial parameter in hypersonic testing in order to match the compressibility effects within the flow. Mach number defines the pressure and temperature ratio across shockwaves along with the angle of shock waves relative to the model. This in turn affects the local temperature and pressure distribution across the surface of the model, if the pressure distribution is not similar it will result in different forces and moments being measured in flight. As Mach number is increased, the realm of 'Mach number independence' is reached. Unfortunately, this cannot be assumed for the current work as the operating Mach number is too low.

The two other pertinent parameters to consider are the mass and mass moment of inertia of the models in relation to the full scale vehicle. This is of great importance when trying to obtain dynamically similar rotations and translations of two bodies relative to one another. Forces and moments acting upon the models are constant as they are only a function of the oncoming flow and the model geometry/attitude. However, the induced translational and rotational accelerations, velocities and displacements will be directly affected by the mass and mass distribution of the models. It is also important to match the relative position of the centre of gravity (CoG) such that rotational motion has the same Moment Reference Centre (MRC).

Table 1: Scaling Groups [11]

Parameter	**Dynamic Similitude Requirements**
Reynolds number	$\frac{v_{full\ scale}}{v_{model}} * \left(\frac{a_{model}}{a_{full\ scale}}\right) * n = 1$
Froude Number	$\left(\frac{a_{model}}{a_{full\ scale}}\right)^2 * \frac{1}{n} = 1$
Mach Number	$M_{model} = M_{full\ scale}$
Length	$l_{model} = n * l_{full\ scale}$
Mass	$m_{model} = \frac{\rho_{f_{model}}}{\rho_{f_{full\ scale}}} * n^3 * m_{full\ scale}$
Moment of Inertia	$I_{model} = \frac{\rho_{f_{model}}}{\rho_{f_{full\ scale}}} * n^5 * I_{full\ scale}$

DOI: 10.13009/EUCASS2017-186

Experimental Setup

4.1 Test Facility

The facility used for these experiments was the University of Southern Queensland's hypersonic wind tunnel (TUSQ). An illustration of this facility is given in Figure 4. This free piston hypersonic shock tunnel provides approximately 200ms of steady flow, with a start-up period of 5ms. It offers an inviscid core flow of 160mm.

For the current study the facility was operated at two different operating conditions. The 'standard condition' with a total pressure of 0.96 MPa and a 'low pressure condition' with a total pressure of 0.58 MPa. The barrel pressure trace for both of these conditions is shown in Figure 5. Further details of the facility and its operation are given in [12].

The ability to operate a facility at multiple conditions is a great advantage when using the free flight technique. Different pressure conditions allow different altitudes to be replicated as this changes the freestream flow density. This combined with changing the inertial properties of the model allows for dynamic similitude of the separation at different points across the vehicle trajectory.

Table 2: TUSQ freestream conditions

	$\mathbf{M_\infty}$	$\mathbf{P_\infty}$	$\boldsymbol{\rho_\infty}$	$\mathbf{T_\infty}$	$\mathbf{U_\infty}$	$\boldsymbol{\gamma}$	$\boldsymbol{\mu}$ **(Sutherland)**	**Re**
Standard Condition	5.81	680 Pa	0.0348 kg/m^3	75 K	985 m/s	1.4	4.66E-6 Pa s	7.15E6 /m
Low Pressure Condition	5.81	454 Pa	0.0243 kg/m^3	65 K	985 m/s	1.4	4.28E-6 Pa s	5.59E6/m

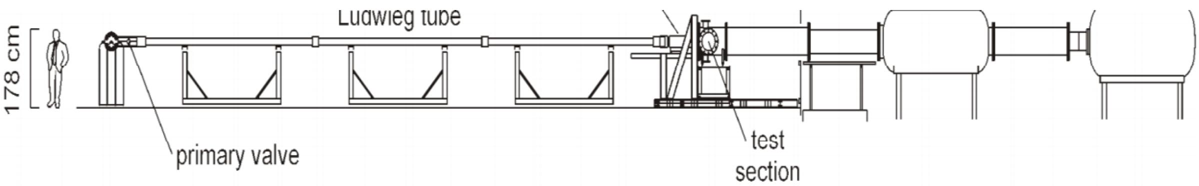

Figure 4: Illustration of TUSQ [12]

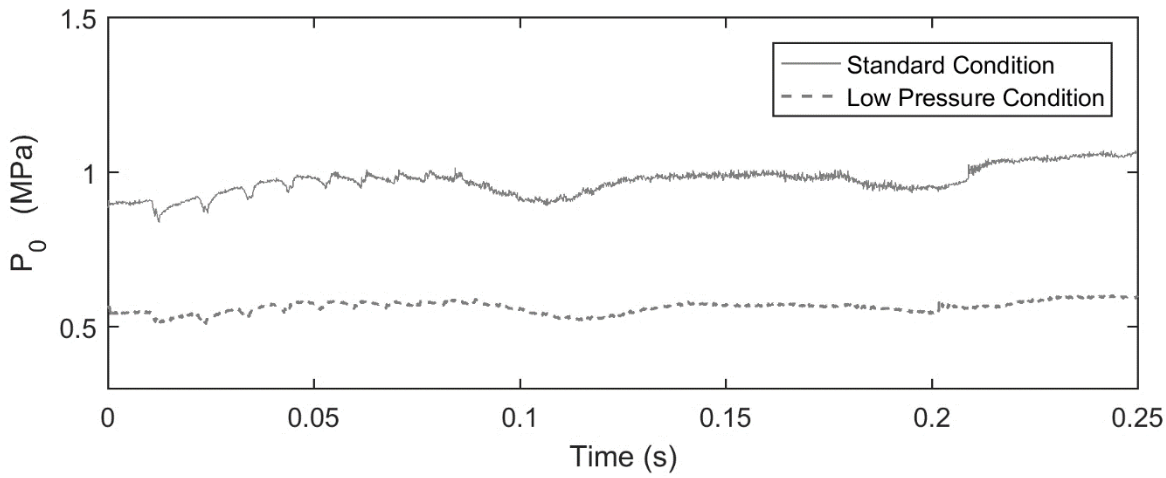

Figure 5: Pressure traces for Standard and Low Pressure conditions

4.2 Model Details

A simplified version of the EFTV/ESM payload was used for the current work, as shown in Figure 6. This reduced complexity geometry was generated for use in numerical and experimental studies to generate an 'idealised' dataset, neglecting effects from fixtures and fittings that appear on the surface. This simplified both the model construction and the complexity of the simulation. The scaling factor for this work was chosen to be 1/13 relative to the full size vehicle. This value was selected based on the size of the inviscid core flow region in the TUSQ facility. Adequate space is required for the model to perform dynamic motions and remain entirely within the core flow region.

DOI: 10.13009/EUCASS2017-186

For practical reasons, a cylindrical sleeve has been added to the rear face of the EFTV around the central umbilical strut to support the ESM whilst the whole assembly is hung by the EFTV on the release assembly prior to the experiment (Figure 7). This fitting has appropriate clearance such that the ESM should not have to overcome any frictional forces holding it in place. It should also be noted that the support struts seen in Figure 3 have been removed. They were found to very brittle when manufacturing at the reduced scale and are believed to have a minimal effect on the overall dynamics of the separation.

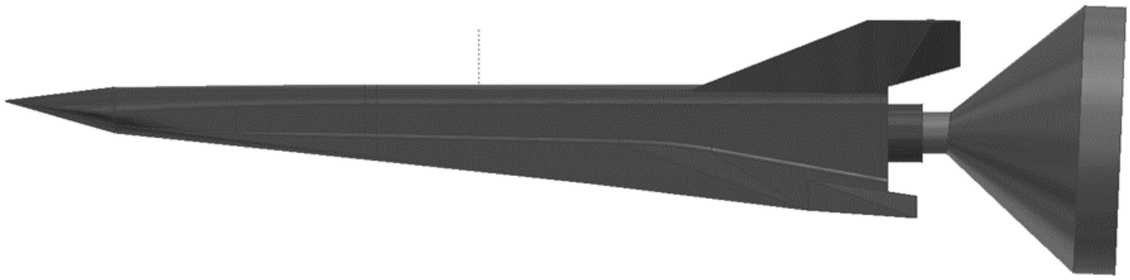

Figure 6: CAD Render of Simplified EFTV+ESM

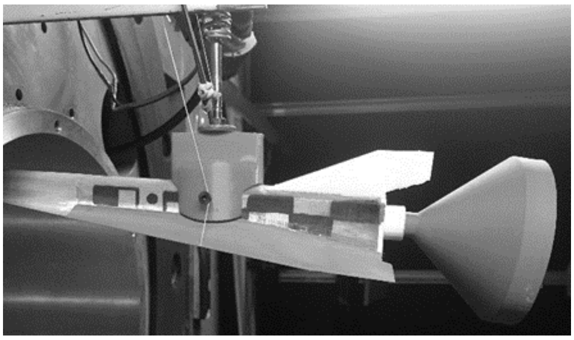

Figure 7: EFTV/ESM assembly being held by the release mechanism prior to an experiment

Models were manufactured by means of 3D printing with poly-lactic acid (PLA) based resin. Two variants were used, regular PLA (ρ = 1.2 kgm^{-3}) and a bronze infused PLA (ρ = 3.5 kgm^{-3}) commercially known as Bronzefill^{TM} produced by ColorFabb. The bronze infused PLA has a much higher density and hence offers much more control over mass distribution of the models and more accurate CoG placement. These structures also have internal cavities to house the on-board instrumentation system and to adjust the inertial properties to better match the scaling requirements.

Table 3 presents the physical properties of the models used and how they compare to the similitude requirements discussed previously. The 'Standard Condition' seeks to replicate the separation dynamics at a flight altitude of 28.2 km. Whereas the 'Low Pressure Condition' is intended to match a 40 km altitude separation, more realistic to what would actually occur on the full scale flight where the separation will take place between 40-60 km.

Table 3: Model Properties

	Standard Condition (0.96 MPa)				**Low Pressure Condition (0.58 MPa)**			
	EFTV		**ESM (Ver01)**		**EFTV**		**ESM (Ver02)**	
	Scaling Target	Achieved	Scaling Target	Achieved	Scaling Target	Achieved	Scaling Target	Achieved
Mass (kg)	0.301	0.304	0.51	0.110	1.31	0.304	0.226	0.223
Ixx (kg mm^2)	111.4	92.72	132.1	39.3	484	92.72	577.7	120.6
Iyy (kg mm^2)	5969.1	5532.7	8657.3	5498.7	25975	5532.7	37877	14654
Izz (kg mm^2)	6006.7	5571.5	8693.7	5498.8	26120	5571.5	38035	14656

Matching the values required for dynamic similitude can in practice be challenging. A large discrepancy can be seen between EFTV scaling targets and what was achieved for the 'Low Pressure Condition'. This was due to the practicalities of making a model heavy enough to meet these requirements and to have that model safely integrate with the release mechanism system. It can be argued that whilst the EFTV mass scaling is poor at this condition, it is in fact a worst case as a heavier model will only reduce the likelihood of aerodynamic coupling between the bodies and potential collision, because of its lower axial acceleration downstream during the free flight test.

DOI: 10.13009/EUCASS2017-186

4.3 Instrumentation

Inertial measurement instruments operate inside both the EFTV and the ESM models. The InvenSense MPU6500 Inertial measurement unit (IMU) sensor was used for acceleration and angular rate measurement. These sensors consist of tri-axial high-speed accelerometers and gyroscopes acquiring data at 8 kHz and 4 kHz respectively. For the current work the full range of each sensor was used +/- 16g and +/ 2000 degrees/s. Freefall detection provided by the accelerometer data was implemented to trigger the system before the onset of the test flow. The custom designed boards feature 32 bit ARM Cortex-M4 processors operating at 72 MHz, 64 K of RAM with 256 K of flash memory. Microcontroller firmware was developed and compiled using the Arduino Integrated development environment. A Class 1 Bluetooth module was included to remotely communicate and control the system whilst it was inside the test facility. The available transmission power offered by the Bluetooth module, along with the extremely close proximity between the EFTV and ESM made it necessary to reduce the transmission power to a level that did not result in interference. Sensor data was stored to volatile memory as it was acquired. Once the instrument's sampling window has closed, data was transferred to non-volatile memory and broadcast by the Bluetooth module to a computer for post-flight analysis. Rechargeable 300 mAh lithium polymer batteries supply power to the system. The instrument offers in-situ charging capability simplifying pre-test procedures before commencing a run. Making use of low power modes in both the microcontroller and Bluetooth module during inactive periods, such as when the test facility is being prepared, makes it possible to use a unit for multiple runs with only a single charge.

Both the EFTV and ESM models have the same instrumentation but tailored layouts of the printed circuit boards (PCB's) to suit the individual geometries. They also both have different batteries to fit within the available internal cavity space. The EFTV instrumentation package is a single long slender PCB that is securely fixed to a tray that sits inside the vehicle fuselage. This is shown in Figure 8. The ESM instrumentation consists of two separate boards with a wired connection between them, this can be seen in Figure 9 and Figure 10. The motherboard consists of the processor and Bluetooth module, along with most of the other major components. The primary component of the daughter board is the IMU, this is placed at axial position closer to the CoG in order to reduce Coriolis effects in the accelerometer measurements.

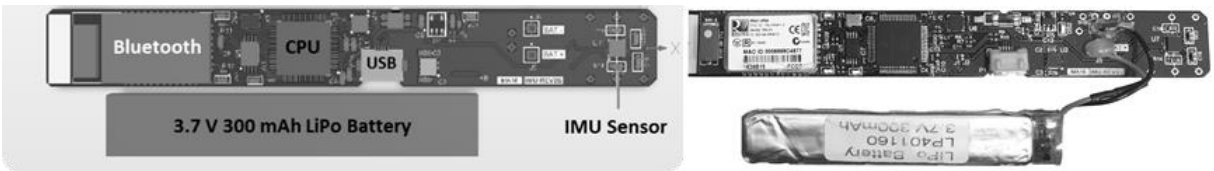

Figure 8: EFTV instrumentation. Render (left) and Photograph (right)

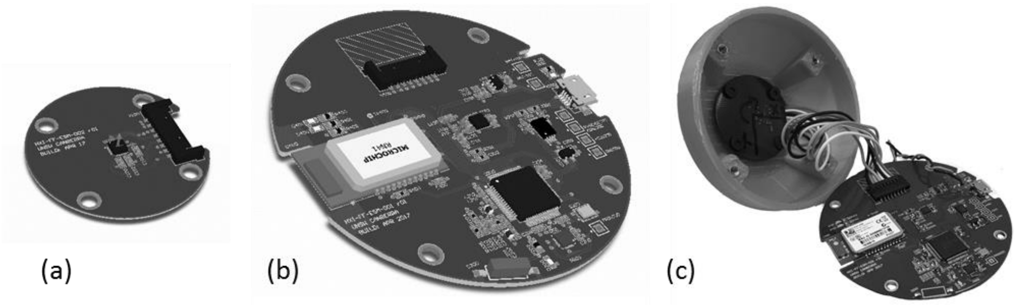

Figure 9: ESM instrumentation package

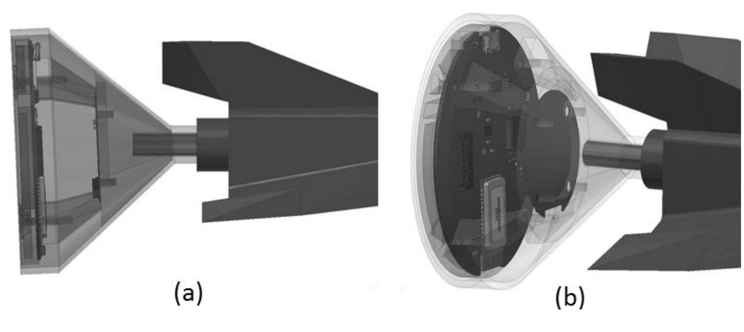

Figure 10: CAD render of ESM with instrumentation on-board

DOI: 10.13009/EUCASS2017-186

4.4 Release Mechanism

Models are released immediately prior to the onset of the flow by means of a thread cutting mechanism. The original version was designed and constructed by [13] but a number of small modifications have been made to increase reliability. An illustration and image of the original system is shown in Figure 11. A clean release is vital as any induced motion, typically roll, can lead to an undesirable starting attitude when flow arrives, which can reduce the usefulness of visualisation data for post-processing. Models are suspended by a single cotton thread tensioned around the base and held against a conformal fitting. 3D printed conformal fittings are designed to hold models securely at a specific starting attitude. An example of the model being held by one of these fittings is shown in Figure 7.

Three actuators are utilised to release the model. These are triggered based on the voltage level of a pressure transducer in the barrel of the facility. An appropriate delay was set such that the model falls to a desirable position when the flow arrives. The first actuator to trigger pushes a platinum tipped razor blade that acts to cut the thread. Once the model has fallen clear of the fitting, the fitting needs to retract to avoid being caught in the test flow. This process involves two actuators. The first moves a small rod that is used to push the fitting down and oppose the force from the tension of the string. A rubber band is also used to ensure the rod is clear. Once the support rod has been removed, a pneumatic actuator retracts the main rod that holds the fitting. A spring is included to prevent fitting impacting the plate that supports the entire mechanism.

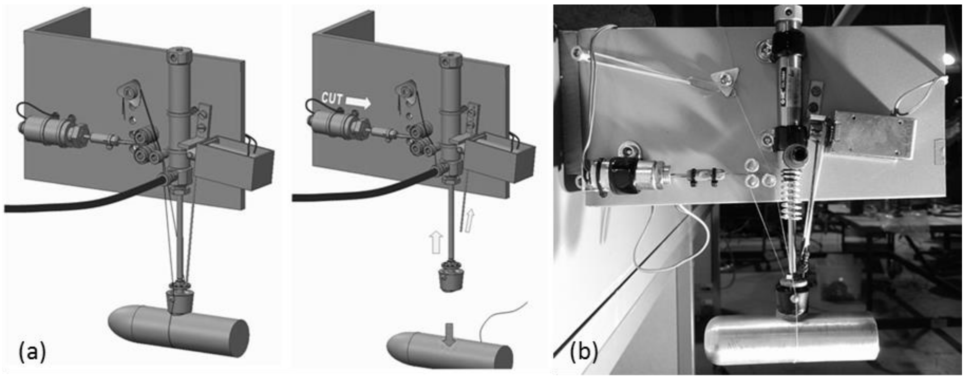

Figure 11: (a) Animation demonstrating the action of the release mechanism. (b) Photo of the actual mechanism. [13]

4.5 Visualisation

A Z-type schlieren system is employed in the current experiments, using a 528 nm LED light source pulsing at 2 kHz with a pulse width of 10 µs. This looks through the side window of the test section to offer a view of the XZ plane of the experiment. There is also a camera view through a window on the top of the test section to inspect motion in the XY plane. Both cameras utilised are Photron Fastcam SA3 Model 120K running at 2000 frames per second (fps). There is also a third camera (Olympus I-SPEED 3) viewing the experiment at 2000 fps and an angle through the horizontal window.

5. Experimental Results

Two experimental runs are analysed in the current work. The first (Run 612) was undertaken at the standard condition of the TUSQ facility with the ESM Ver01 model. With regard to similitude, this is attempting to reproduce the separation dynamics of a 29 km altitude separation. The second experiment (Run 620) was performed at the 'low pressure' condition of the facility with the ESM Ver02 model. Both experiments used the same EFTV model. Figure 12 and Figure 13 show selected frames from the three high speed cameras recording the experiment that took place during Run 612 and Run 620 respectively of the TUSQ facility. It should be noted that these images are on different time scales as the separation takes place much more rapidly in Run 612. It can be seen in both cases studied the EFTV motion can be considered minimal relative to that of the ESM.

DOI: 10.13009/EUCASS2017-186

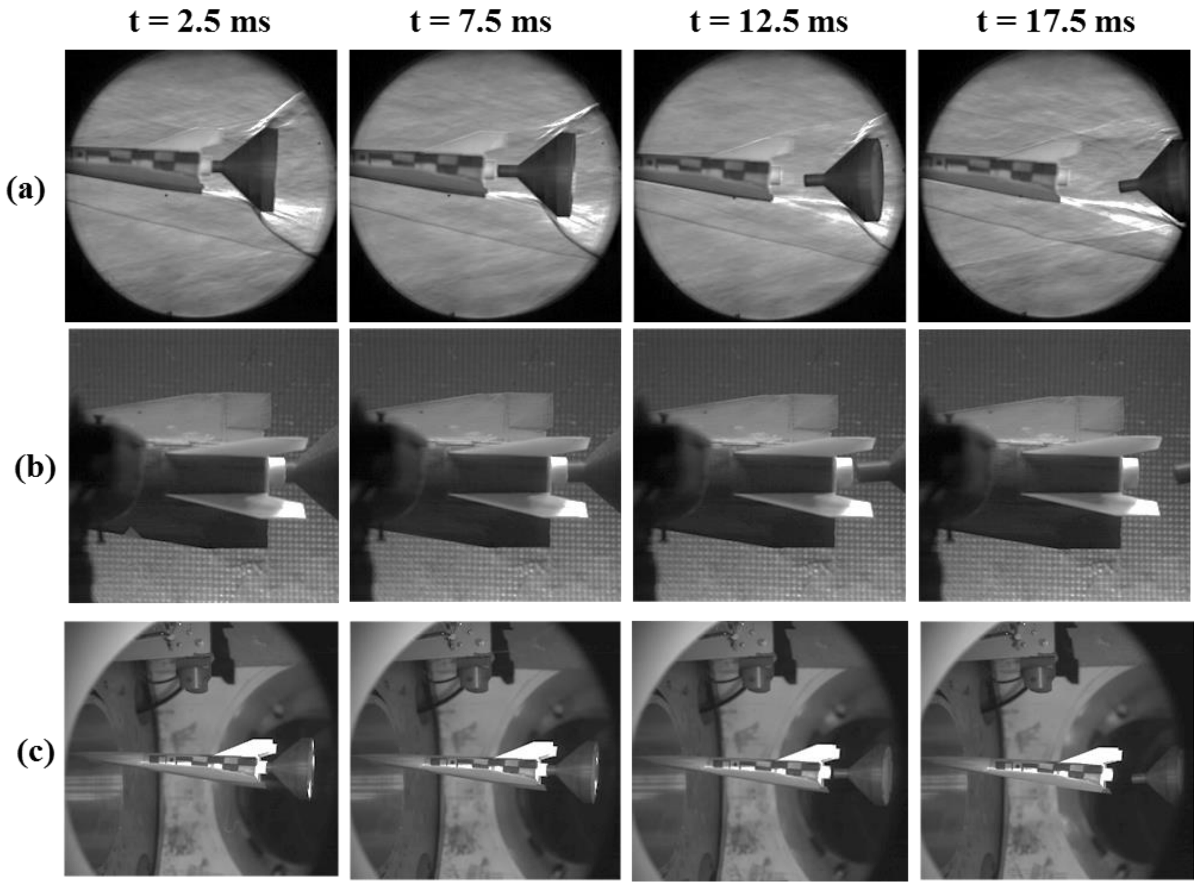

Figure 12: Selected frames from Run 612 (a) schlieren (b) top view high speed camera (c) angled side view high speed camera

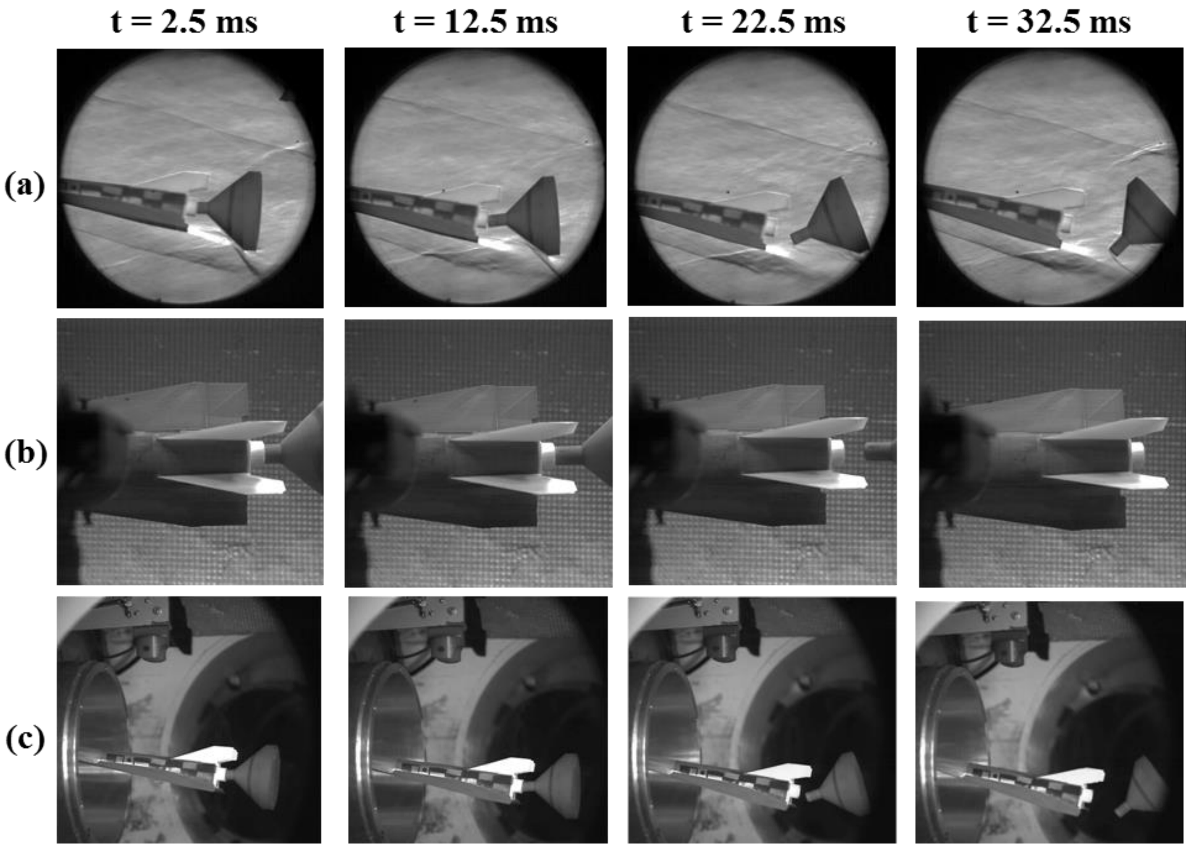

Figure 13: Selected frames from Run 620 (a) schlieren (b) top view high speed camera (c) angled side view high speed camera

DOI: 10.13009/EUCASS2017-186

5.1 Sensor Data

On-board instrumentation on both the EFTV and ESM acquired data from an inertial measurement unit during experimental Run 620. These systems consist of accelerometers and gyroscopes to measure accelerations and angular velocities respectively. Data from these sensors is shown in Figure 14. These measurements are in the local coordinate frame of the model and as such need to be transformed into fixed global reference frame relative to the flow direction.

Some issues were experienced with sensor saturation during the experimental runs. Run 612 operated at the 'standard pressure' condition in which ESM Ver01 accelerated away from the EFTV at a rate exceeding the limits of the IMU measurement system. This acceleration was calculated from the schlieren footage to be approximately 24g. To negate this, ESM Ver02 was conceived. Instead of regular PLA this version was produced using the bronze infused PLA to increase mass and hence reduce the acceleration into the range which the sensor can measure. To further reduce the drag force, the facility was operated at the 'low pressure' condition. These modifications were made in conjunction with calculating how this affected the dynamic scaling parameter. ESM Ver02 along with the 'low pressure' condition sought to replicate a full scale flight altitude of 40 km.

Accelerations of both the ESM and EFTV models can be seen to remain within the range of the sensor for the duration of the separation. Transverse acceleration was seen to be minimal for both models. Vertical and axial acceleration components of the ESM vary as the model rotates relative to the test flow. The EFTV model is shown to generate a nominally constant amount of lift as its attitude changes minimally during the separation. A sharp pitching motion is experienced by the ESM which can be seen in the gyroscope reading which experiences saturation before the end of the experiment. Thankfully this occurs after the separation has taken place. Angular motion of the EFTV is seen to be minimal.

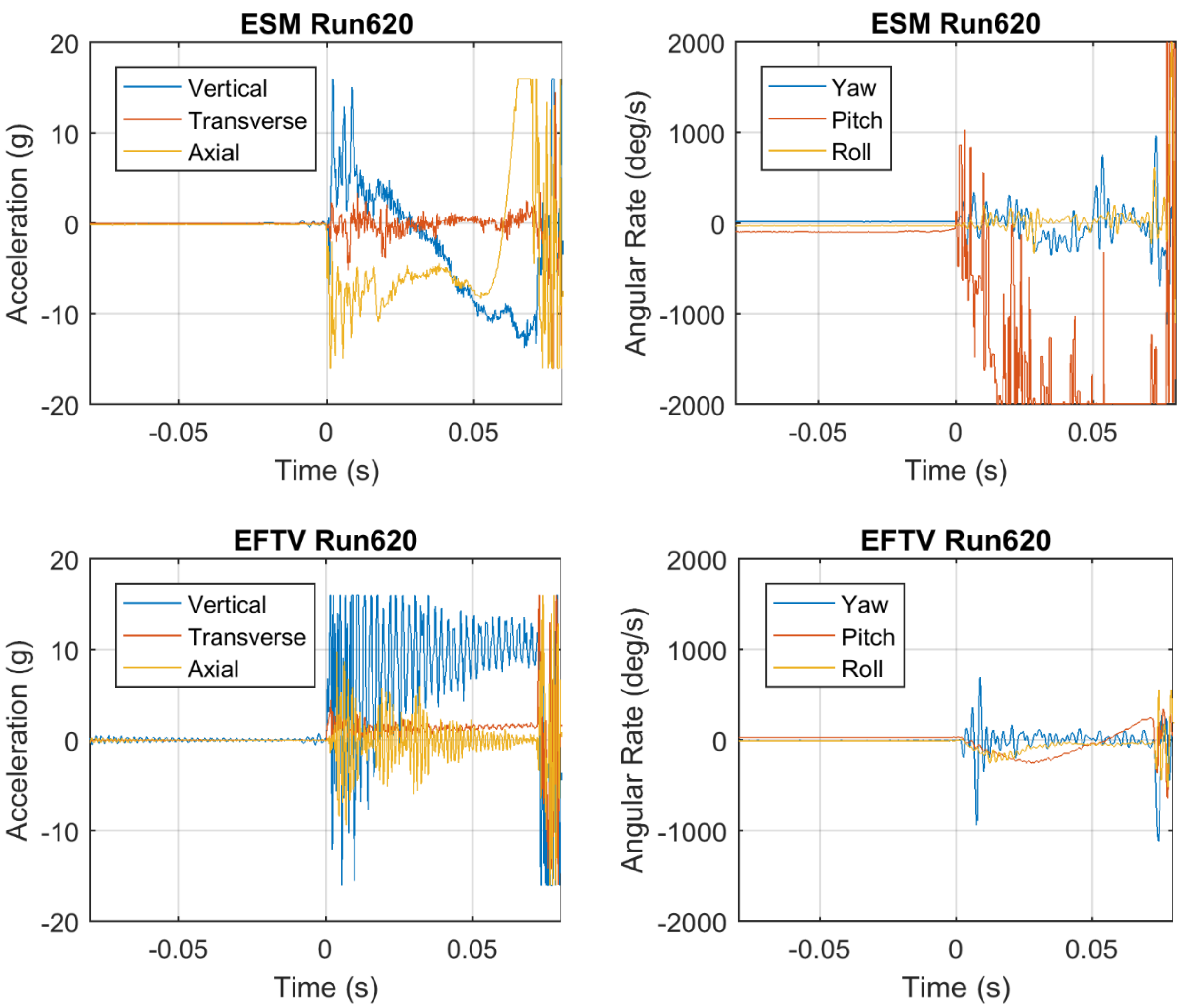

Figure 14: EFTV/ESM IMU Data (Model Frame)

DOI: 10.13009/EUCASS2017-186

5.2 Image Processing

Two techniques were utilised to obtain trajectory of the ESM relative to the EFTV. In Run 620 where lateral motion (yaw/roll) was limited, edge detection was used to track the back face of the ESM. An intensity threshold was imposed to give the location of this edge compared to the background. A first order polynomial is then applied fit to the points and comparing lines frame to frame yields displacements and rotations. This can be seen in Figure 15.

The second technique utilised is based on feature detection. Unique pixel groups are detected and are matched with their corresponding location on the adjacent frame. From this rotation and translation data can be calculated. An example of feature detection between two frames on the ESM during Run 612 is shown in Figure 16.

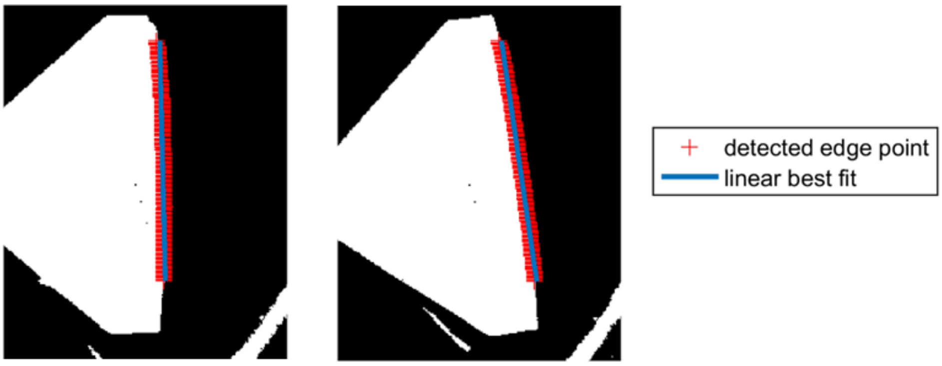

Figure 15: Edge tracking example frames. Frame 280 (left), Frame 290 (right)

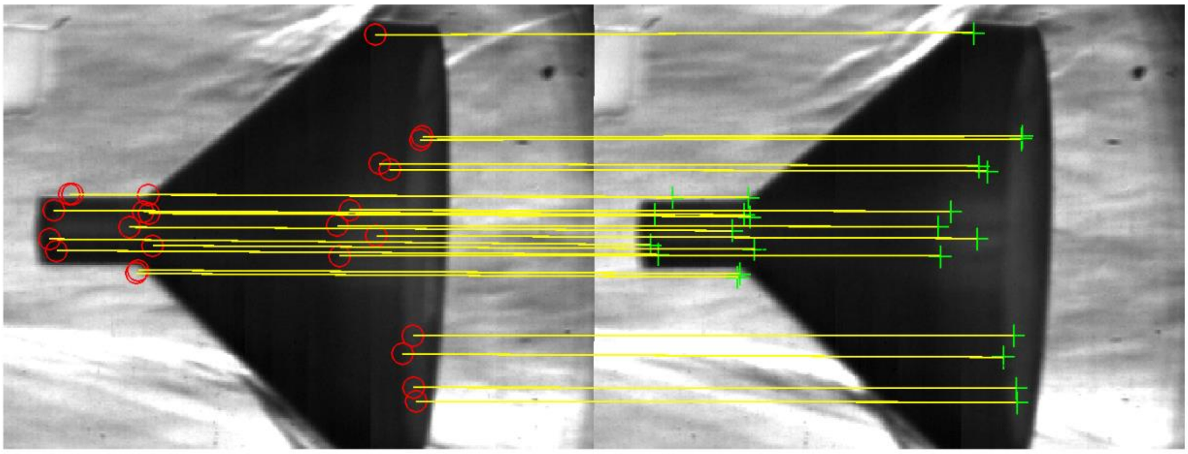

Figure 16: Feature detection between adjacent frames on Run 612

6. Numerical Simulation

6.1 DLR TAU code

For the numerical simulation the DLR in-house code TAU developed by the Institute of Aerodynamic and Flow Technology of the German Aerospace Center (DLR) has been used. The TAU flow solver [14] uses the finite volume method to discretize Euler or Navier-Stokes equations on unstructured grids. Based on this primary grid an edge-based metric called dual-grid is generated in a pre-processing step. If multi-grid technique is used, the pre-processor also agglomerates coarser levels of the dual-grid. Also domain splitting is done by the pre-processor in case of parallel computations.

For supersonic cases the Computational Fluid Dynamics (CFD) solver module compute inviscid terms employing an AUSMDV upwind scheme with linear reconstruction to achieve second-order spatial accuracy. Viscous terms are generally computed with a second-order central scheme. For time integration various explicit Runge-Kutta schemes, as well as an implicit approximate factorization lower-upper symmetric Gauss-Seidel scheme (LU-SGS) is implemented. For time accurate computations a Jameson-type dual time stepping approach is employed. Additional convergence acceleration is achieved by explicit residual smoothing.

DOI: 10.13009/EUCASS2017-186

For moving grids TAU is written in an arbitrary Eulerian-Lagrangian formulation. The technique of overlapping grids (Chimera technique) [15] is applied to simulate configurations with movable parts. The method handles the data exchange in the overlapping region of the computational domains of each part. For simulations with moving bodies the motion is separately solved in the Rigid Body Dynamics (RBD) module solving Newton's second law and the Euler equation of rotational dynamics. The coupled CFD/RBD problem is solved in a partitioned manner. A so-called strong coupling scheme is used [16]. Strong coupling means that the coupled equations are iteratively solved within every physical time step by repeatedly solving the involved disciplines CFD and RBD separately based on the exchanged coupling quantities. These are on CFD side aerodynamic loads (forces and moments) and on RBD side the motion state (position and velocities).

The inviscid simulation of the EVTV/ESM separation was carried out on a numerical grid with 83.3 million tetraeders (18.9 million points). Figure 17 shows the computational domain after 200 time steps (t=1s). Shown is the EFTV in blue, ESM in green and the far field boundary for each part in grey.

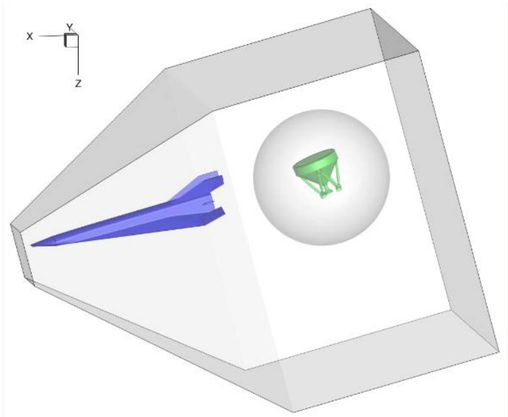

Figure 17: Computational domain for CFD/RBD simulations

6.2 Simulation Results

The results of two simulations are shown in Figure 18 and Figure 19. The first is a simulation of experimental run 612 and the second is a simulation of the full scale scenario. The full scale case was simulated at an altitude of 55 km, M = 6.9, 2.6˚ angle of attack, 20˚ flap angle and a -18.3˚ flight path angle (FPA). It should be noted that this is a substantially different case than the one studied in the experimental work and is intended to be a prediction of behaviour during the real flight. FPA is the most challenging to replicate due to the velocity of subscale model being orders of magnitude less than that of the flow velocity.

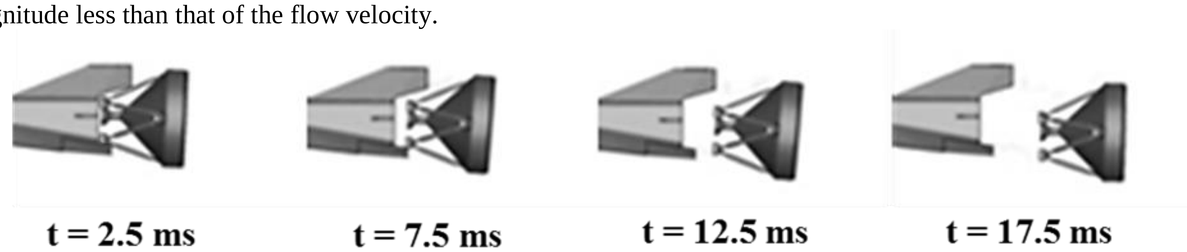

Figure 18: Simulation of subscale experiment. TUSQ Standard Condition, M 5.8, AoA 0˚, FPA 0˚, Flap 0˚.

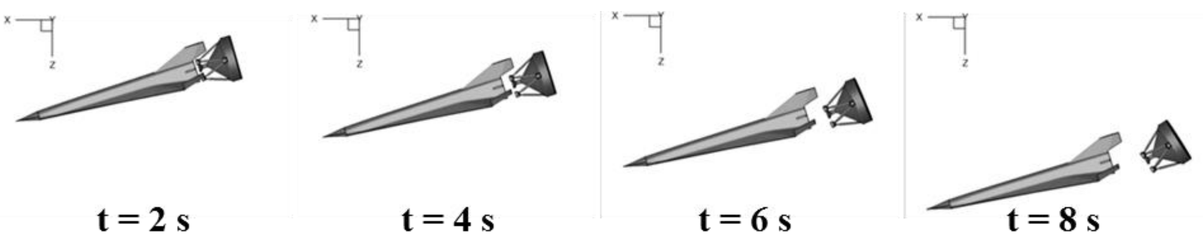

Figure 19: Full Scale simulation (55 km altitude) 55 km, M 6.9, AoA 2.6˚, FPA -18.3˚, Flap 20˚.

DOI: 10.13009/EUCASS2017-186

7. Comparison of Results

This section presents a comparison of all the results gathered from both experimental and numerical studies of the EFTV and ESM separation. Figure 20 shows the results of the coupled CFD/RBD simulation for the full scale vehicle. Clearly this separation occurs at a fundamentally different timescale than that of the subscale experiments due to increased mass and inertia present. However, the overall trend can still be observed.

Figure 21 displays both the results from the image analysis of Run 612 and subscale CFD/RBD simulations. Angular motion is similar but delayed by approximately 5 ms. The simulation predicts a slight increase in pitch angle before the major drop, however this is absent from the experiment. This is thought to be a function of sleeve fitting that was added to the EFTV model to support the ESM prior to the experiment. The sleeve may be preventing this initial upwards pitch and once the ESM is free of the constraint, the movement is dominated by the pressure on the upper surface causing the nose down rotation. Displacements in the X direction agree within duration of the separation, as the ESM as detached by roughly 10 ms. As the displacement is calculated frame to frame, any slight measurement error will accumulate as the model is tracked for longer time durations.

Figure 22 shows motion data captured from the ESM Ver02 during Run 620 at the ‘low pressure’ condition. In this case the downwards pitching motion is much more prevalent. Rotation occurs almost immediately without the preceding plateau that occurred in the previous two cases. Rotation data from both image analysis and integrated gyroscope measurements show good agreement.

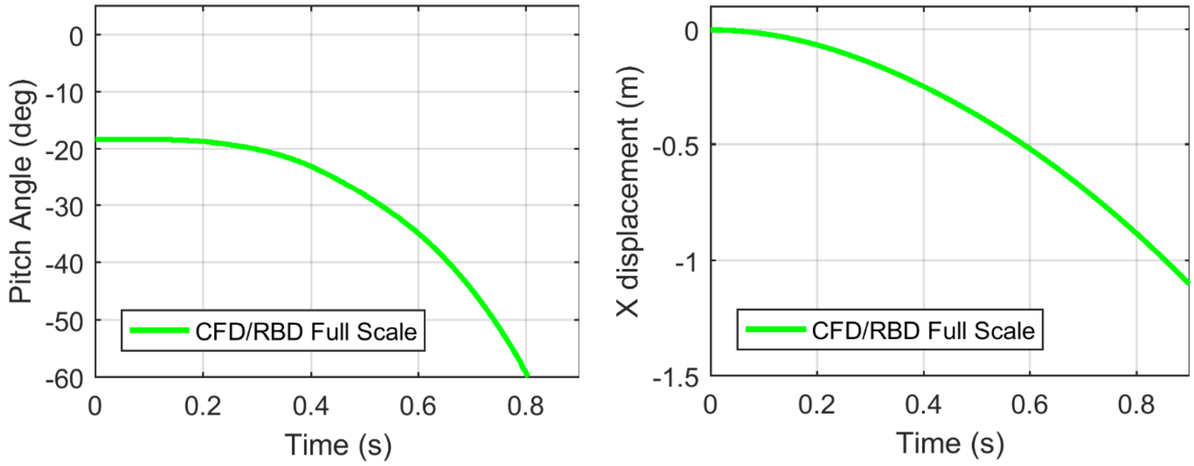

Figure 20: ESM motion. Full Scale CFD/RBD.

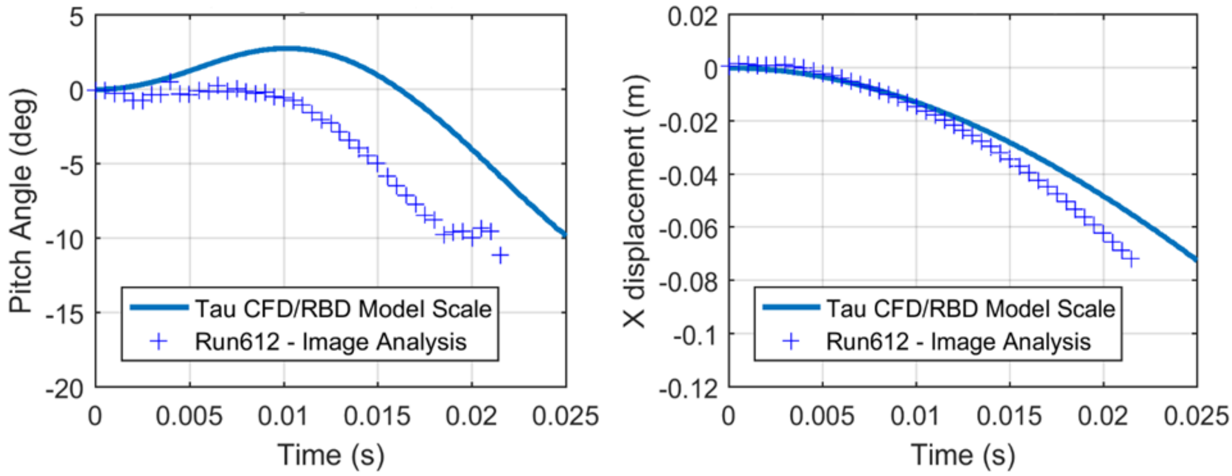

Figure 21: ESM motion. Experimental run 612 and Subscale CFD/RBD simulation

DOI: 10.13009/EUCASS2017-186

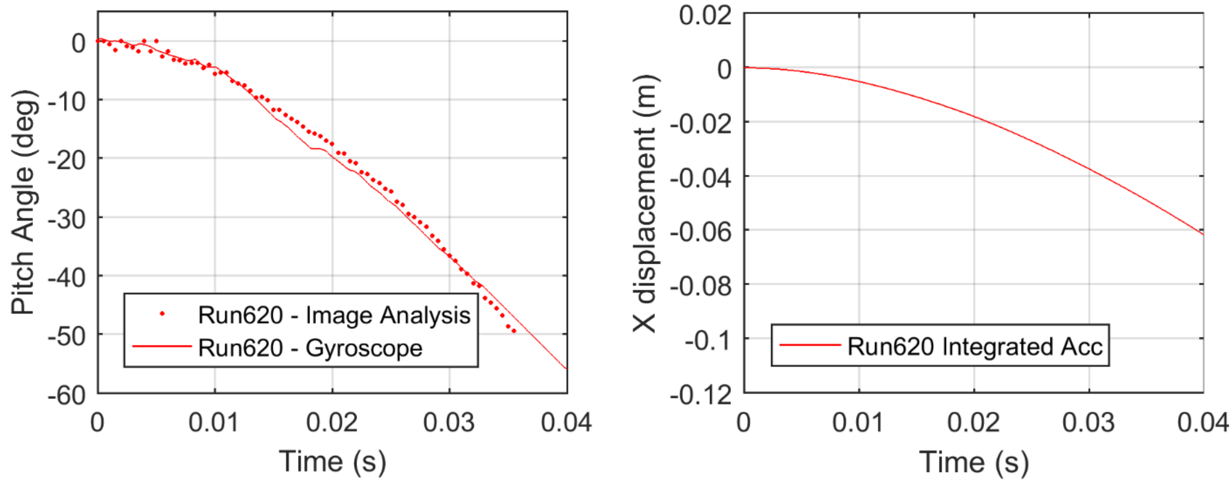

Figure 22: ESM motion. Experimental run 620.

8. Conclusions

This study has shown that it is possible to extract quantitative information regarding the separation dynamics of two bodies using the free flight technique. A combination of on-board instrumentation and analysis of high-speed video footage have been used to determine the separation dynamics of the HEXAFLY-INT experimental flight test vehicle and a support module. Experiments were conducted on subscale models and results compared with coupled CFD/RBD numerical simulations. Similar trends were observed in the overall dynamics of the separation. However, further numerical and experimental work needs to be performed to more directly compare the results and establish whether the separation in the real test flight will occur safely.

9. Acknowledgements

This work is performed within the ‘High Speed Experimental Fly Vehicles - International’ (HEXAFLY-INT) project fostering International Cooperation on Civil High-Speed Air Transport Research. HEXAFLY-INT, coordinated by ESAESTEC, is supported by the EU within the 7th Framework Program Theme 7 Transport, Contract no.: ACP3-GA-2014-620327. The project is also supported by the Ministry of Industry and Trade, Russian Federation. Further information on HEXAFLYINT can be found on http://www.esa.int/techresources/hexafly_int.
The authors would also like to thank electronics engineer Liam McQuellin for his hard work redeveloping the on-board instrumentation packages.

10. References

[1] Mee, D. J., Daniel, W. J. T. and Simmons, J. M., “Three-component force balance for flows of millisecond duration,” AIAA Journal, 34(3) 590-595, 1996.

[2] Mudford, N. R., O'Byrne, S., Balage, S., and Neely, A. J., “Hypersonic Wind Tunnel Free Flying Experiments with Onboard Instrumentation,” AIAA Journal of Spacecraft and Rockets, October 2014.

[3] Kennell, C., Neely, A.J., O’Byrne, S., Buttsworth, D. “Measurement of Vehicle Stability Coefficients in Hypersonic Wind Tunnels,” 20th AIAA International Space Planes and Hypersonic Systems and Technologies Conference, Glasgow, July 2015.

[4] Kennell C, Neely A, Tahtali M, Buttsworth DR, Choudhury R., “Free Flight Testing in Hypersonic Flows: HEXAFLY-INT EFTV”, AIAA 2016-1088, AIAA SciTech, January 2016.

[5] S. J. Laurence, N. J. Parziale, and R. Deiterding, “Dynamical separation of spherical bodies in supersonic flow”, Journal of Fluid Mechanics, 713:159-182, 2012.

DOI: 10.13009/EUCASS2017-186

[6] Steelant, J., Langener, T., Hannemann, K., Marini, M., Serre, L., Bouchez, M., Falempin, F., "Conceptual Design of the High-Speed Propelled Experimental Flight Test Vehicle HEXAFLY", 20th AIAA International Space Planes and Hypersonic Systems and Technologies Conference, International Space Planes and Hypersonic Systems and Technologies Conferences, (AIAA 2015-3539)

[7] Steelant, J., Varvill R., Defoort S., Hannemann K. and Marini M., “Achievements Obtained for Sustained Hypersonic Flight within the LAPCAT-II project.” 20th AIAA International Space Planes and Hypersonic Systems and Technologies Conference, July Glasgow, Scotland. 2015.

[8] Steelant J., “ATLLAS: Aero-Thermal Loaded Material Investigations for High-Speed Vehicles”, 15th AIAA International Space Planes and Hypersonic Systems and Technologies Conference, 28/04-01/05-2008, Dayton, Ohio, USA, AIAA-2008-2582

[9] Favaloro, N., Pezzella, G., Carandente, V., Scigliano, R., Vitale, A., Rispoli, A., Steelant, J., “Design Analysis of the High-Speed Experimental Flight Test Vehicle HEXAFLY-International”, 20th AIAA International Space Planes and Hypersonic Systems and Technologies Conference, July Glasgow, Scotland. 2015. AIAA-2015-3607. doi: 10.2514/6.2015-3644.

[10] Steelant, J., Chernyshev, L., Kallenbach, A., Grigoriev, N., Wagner, A., Prokhorov, A., Andro, J.-Y., Gubanov, A., Neely, A., Verstraete, D., Di Benedetto, S., Voevodenko, N., Saracoglu, B., Vyshinsky, V, “HEXAFLY-INT: Periodic Reporting of Period II”. EC Report

[11] Chester H. Wolowicz, James S. Bowman, Jr., and William P. Gilbert “Similitude Requirements and Scaling Relationships as Applied to Model Testing,” NASA Technical Paper 1435, August 1979.

[12] Buttsworth, D. R., “Ludwieg Tunnel Facility with Free Piston Compression Heating for Supersonic and Hypersonic Testing,” 9th Australian Space Science Conference 2009, Published 2010.

[13] Kistemaker, B. “Development of an improved free flight model release mechanism for the TUSQ hypersonic wind tunnel,” BEng project report, 2014.

[14] Schwamborn, D., Gerhold, T. & Heinrich, R., The DLR TAU-Code: Recent Applications in Research and Industry, ECCOMAS 2006, Delft, The Netherlands, 2006.

[15] Madrane, A., Heinrich, R. & Gerhold T.,Implementation of the chimera method in the unstructured hybrid DLR fine volume TAU-code,6th Overset Composite Grid and Solution Technology Symposium, Ft. Walton Beach, USA, 2002.

[16] Reimer, L., Heinrich, R. & Meurer, R., Validation of a Time-Domain TAU-Flight Dynamics Coupling Based on Store Relation Scenarios, Notes on Numerical Fluid Mechanics an Multidisciplinary Design, 455--463, Springer, 2014.